


Localization and spin dynamics of spin-orbit-coupled Bose-Einstein condensates in deep optical lattices

Ai-Xia Zhang, Xiao-Wen Hu, Yan-Fang Jiang, Jun-Cheng Liang, Ying Zhang , Wei Zhang, and Ju-Kui Xue 
College of Physics and Electronic Engineering, Northwest Normal University, Lanzhou 730070, China

 (Received 2 July 2021; revised 28 October 2021; accepted 9 December 2021; published 28 December 2021)

We analytically and numerically discuss the dynamics of two pseudospin components Bose-Einstein condensates (BECs) with spin-orbit coupling (SOC) in deep optical lattices. Rich localized phenomena, such as breathers, solitons, self-trapping, and diffusion, are revealed and strongly depend on the strength of the atomic interaction, SOC, Raman detuning, and the spin polarization (i.e., the initial population difference of atoms between the two pseudospin components of BECs). The critical conditions for the transition of localized states are derived analytically. Based on the critical conditions, the detailed dynamical phase diagram describing the different dynamical regimes is derived. When the Raman detuning satisfies a critical condition, localized states with a fixed initial spin polarization can be observed. When the critical condition is not satisfied, we use two quenching methods, i.e., suddenly and linearly quenching Raman detuning from the soliton or breather state, to discuss the spin dynamics, phase transition, and wave packet dynamics by numerical simulation. The sudden quenching results in a damped oscillation of spin polarization and transforms the system to a new polarized state. Interestingly, the linear quenching of Raman detuning induces a controllable phase transition from an unpolarized phase to an expected polarized phase, while the soliton or breather dynamics is maintained.

DOI: [10.1103/PhysRevE.104.064215](https://doi.org/10.1103/PhysRevE.104.064215)

I. INTRODUCTION

Spin-orbit coupling (SOC), the interaction between the spin of a quantum particle and its orbital motion, significantly overlaps with traditional condensed matter phenomena, but more importantly, it could also contain new phenomena, such as spin Hall effects [1], topological insulators and superconductors [2,3], etc. The recent experimental realization of one-dimensional (1D) [4–6] and two-dimensional (2D) [7–9] SOC in ultracold atoms provides a powerful control knob in quantum gases for exploring nontrivial topological physics induced by SOC and has opened up a new avenue for studying the rich SOC physics in Bose-Einstein condensates (BECs) [6,10–17]. Different couplings such as Rashba [18] and Dresselhaus [19], as well as a mixture of them [20], have been realized. In BEC systems, the effective SOC stemming from internal atomic states which are coupled by Raman laser fields [21] can be tuned by means of fast and coherent modulations of the laser intensities [22]. This can be achieved via modulation of the Raman term, as experimentally demonstrated, by modulating gradient magnetic fields [23,24], or by time-periodic modulation of the Zeeman field [15]. On the other hand, multicomponent BECs are an ideal system for investigating phase transitions. The realization of one-dimensional SOC [4] in a two-component BEC brings out a novel dispersion relation. This dispersion relation is characterized by two energy bands with a double-well structure in the lower branch. In this case, the ground-state phase diagram [25–28] and the collective excitation [29–31] are greatly enriched by this special dispersion.

Another important typical potential engineered in BECs is optical lattices. BECs trapped in the periodic optical potential

have been attracting growing interest in view of the value of studying fundamental and applied aspects of quantum optics, quantum computing, and solid state physics [32–36]. Optical lattices provide a clean, many-particle system with enhanced atomic interactions, and they are a powerful tool for studying the quantum behavior of periodic systems. BECs loaded into optical lattices produce extremely rich dynamics and provide a versatile test bed for studying the localization phenomena [37–39]. To date, localization phenomena have been observed in many physical systems, including spin chains [40], periodically curved arrays of optical wave guides [41,42], and cold atoms loaded in shaken optical lattices [43]. Discrete breathers have been observed experimentally in various physical systems such as nonlinear wave guides arrays [44,45], Josephson junctions [46,47], and BECs in optical lattices [48]. On the other hand, self-trapping has been studied theoretically in all dimensions [49–52] and experimentally in double-well systems [53] and in arrays of 2D pancakelike BECs created by a deep 1D lattice potential [54]. There are many different methods and experimental technologies to generate solitons in BECs, which has allowed both bright and dark solitons to be extensively investigated [55–64]. In multicomponent BECs, the high number of degrees of freedom leads to a rich localization dynamics [65–68]. The localized states of ultracold atomic gases provide a key avenue for stable output of matter waves, which has important application prospects in many high-tech fields [69]. Because of the rich coupling dynamics of ultracold atomic gases, the localization phenomenon in ultracold atomic gases not only opens up a new research field in nonlinear physics but also provides a new platform for studying atomic fluctuations [70]; what is more, it is convenient for people to have a deep understanding of its formation mechanism and inherent dynamical characteristics [71].

The combination of SOC and optical lattices in BECs is particularly intriguing. In recent years, the properties of gap solitons in spin-orbit-coupled BECs in one- and two-dimensional spin-dependent optical lattices have been studied, and it was demonstrated that gap solitons can be categorized according to their spin-dependent parity and time-reversal and translational symmetries [72,73]. The existence and stability of different types of discrete solitons of spin-orbit-coupled BECs in optical lattices have been demonstrated [74]. The coexistence and properties of stable compact localized states and discrete solitons for binary BECs with SOC loaded in optical lattices have been reported [75]. It is important to control the localization properties of the ground state of a BECs mixture in a deep optical lattice by means of the SOC parameter [15]. Recently, dynamical localization of binary mixtures of BECs with SOC subjected to a deep optical lattice was investigated [76]. However, in spin-orbit-coupled BECs exposed to deep optical lattices, due to the interplay between SOC, periodicity, and nonlinearity, rich localized states should occur, such as self-trapping, breathers, and diffusion, which are still open issues. Especially, the critical condition for the transition among the different localized states is not clear.

In this paper, we investigate the localization phenomena of two-component BECs with SOC in deep optical lattices, focusing on the effect of SOC strength and Raman detuning on the transition of the localization. First, from the tight-binding model with the mean-field approximation, we derive a discrete nonlinear Schrödinger equation. To study various dynamical regimes, we consider the evolution of a Gaussian profile wave packet and use the variational method for analytical understanding of the localized states. By solving the Euler-Lagrange equations, the variational equations of motion can be derived. Based on them, the transition critical condition of localized states without an exchange of atoms between the two pseudospin components is discussed. Rich localized phenomena, such as diffusion, solitons, breathers, and self-trapping, are revealed. According to the critical conditions, the dynamical phase diagrams are derived. Then the analytical predictions are confirmed by direct numerical simulations of the full discrete nonlinear Schrödinger equation describing the system. We also study the localized states with an exchange of atoms between two pseudospin components numerically via quenching of the Raman detuning. The spin dynamics can be excited by suddenly and linearly quenching the Raman detuning from the soliton or breather state. Correspondingly, the polarization and the soliton dynamics of the system will be modified. Particularly, linear quenching of Raman detuning results in a controllable phase transition from the unpolarized phase to an expected polarized phase, while the soliton or breather is maintained. SOC and Raman detuning play important roles in the dynamics of the BECs in deep optical lattices. With a change in SOC and Raman detuning strength, different localized states will occur.

This paper is organized as follows: in Sec. II, we briefly introduce the theoretical model and some essential ideas used in the theoretical treatment of BECs with SOC in deep optical lattices and derive the differential equations of motion by using the variational method. Then, Secs. III and IV discuss the localized states and corresponding spin dynamics without

and with an exchange of atoms between two pseudospin components, respectively. Section V gives a summary of the work.

II. MODEL AND VARIATIONAL APPROACH

We consider a mixture of two-component spin-orbit-coupled BECs in one-dimensional optical lattices. The atoms of the BECs are exposed to three laser fields in a tripod-type linkage pattern [39,77]. By controlling the corresponding wave number k_R of lasers, the atoms are characterized by a manifold of three ground states, $|1\rangle$, $|2\rangle$, and $|3\rangle$, coupled to a common excited state $|0\rangle$. Two of the control lasers are counterpropagating along the x axis with Rabi frequencies ω_1 and ω_2 , whereas the third laser propagates along the y axis with Rabi frequency ω_3 , and $\omega = \sqrt{\sum_{i=1}^3 |\omega_i|^2}$ denotes the total Rabi frequency. The tripod scheme generates an effective spin-1/2 system with the spin-orbit-coupled single particle Hamiltonian $H_0 = -\sum_{i=1}^3 (\hbar\omega_i |0\rangle\langle i| + \text{H.c.})$ [39]. This Hamiltonian has two degenerate dark states, $|D_1\rangle$ and $|D_2\rangle$, and a general state $|\Phi(\mathbf{r})\rangle$ can be expanded in terms of the dark states as $|\Phi(\mathbf{r})\rangle = \sum_{j=1}^2 \psi_j(\mathbf{r}) |D_j(\mathbf{r})\rangle$, where components ψ_\uparrow and ψ_\downarrow represent the wave functions of the two dark states emulating pseudospins $|\uparrow\rangle$ and $|\downarrow\rangle$. The dynamics of the system is governed by the coupled Gross-Pitaevskii equation [72,77],

$$i\hbar \frac{\partial \Psi}{\partial t} = H\Psi, \quad (1)$$

where $\Psi = (\psi_\uparrow, \psi_\downarrow)^T$. The total Hamiltonian $H = H_0 + H_{\text{int}}$. H_0 is the spin-orbit-coupled single particle Hamiltonian; H_{int} denotes the two-body atomic interactions. H_0 can be written as

$$H_0 = \frac{k_x^2}{2m} + \chi^* k_x \sigma_x + \hbar\tilde{\Omega} \sigma_z + V_{\text{OL}}(x), \quad (2)$$

where $k_x = -i\hbar\partial/\partial x$ is the momentum operator, m is the mass of the atom. $\tilde{\Omega}$ is the two photo Raman detuning induced by the frequency of the Raman lasers and the Zeeman splitting, which can be changed by adjusting the applied magnetic field independently. The SOC strength, accounted for by coefficient $\chi^* = \hbar k_R/m$, results from a combined effect of the Rashba and Dresselhaus couplings, which is determined by intensities and wavelengths of laser beams. σ_x, σ_z are the Pauli matrices. $V_{\text{OL}}(x) = V_0 \cos(2k_L x)$ (k_L is the lattice wave number) is optical lattice potential, which can be generated by two counterpropagating laser fields. Under the mean-field approximation, H_{int} has the following form:

$$H_{\text{int}} = 2\omega_\perp \hbar \times \text{diag}(a_{\uparrow\uparrow} |\psi_\uparrow|^2 + a_{\uparrow\downarrow} |\psi_\downarrow|^2, a_{\downarrow\downarrow} |\psi_\downarrow|^2 + a_{\downarrow\uparrow} |\psi_\uparrow|^2), \quad (3)$$

where $a_{\uparrow\uparrow}$ ($a_{\downarrow\downarrow}$) and $a_{\uparrow\downarrow}$ are the s -wave scattering lengths of the condensates and we assume $a_{\uparrow\uparrow} = a_{\downarrow\downarrow} = a$ [15].

The physical variables are rescaled as $\psi_j \sim \sqrt{\omega_R/2\omega_\perp a_0} \psi_j$, $x \sim k_L^{-1} x$, $t \sim t/\omega_R$, $\Omega \sim \tilde{\Omega}/\omega_R$, $\tilde{\chi} \sim 2\chi^*/k_L$, $V_{\text{OL}}(x) \sim V(x)E_R = V_0 \cos(2x)E_R$, and $\tilde{g} = a/a_0$ and $\tilde{g}_{\uparrow\downarrow} = a_{\uparrow\downarrow}/a_0$ are, respectively, the dimensionless intra- and interinteractions, where ω_\perp is the trapping frequency along the transverse direction, $\omega_R = \hbar k_R^2/2m = E_R/\hbar$, E_R is the recoil energy of Raman lasers, and a_0 is the Bohr radius [15].

Then we obtain the dimensionless Gross-Pitaevskii equation

$$i\frac{\partial\psi_{\uparrow,\downarrow}}{\partial t} = -\frac{\partial^2\psi_{\uparrow,\downarrow}}{\partial x^2} - i\tilde{\chi}\frac{\partial\psi_{\downarrow,\uparrow}}{\partial x} - (-1)^j\Omega\psi_{\uparrow,\downarrow} + V(x)\psi_{\uparrow,\downarrow} + (\tilde{g}|\psi_{\uparrow,\downarrow}|^2 + \tilde{g}_{\uparrow\downarrow}|\psi_{\downarrow,\uparrow}|^2)\psi_{\uparrow,\downarrow} \quad (j = 1, 2). \quad (4)$$

For a sufficiently deep optical lattice potential, the BECs are considered to be weakly coupled and isolated, so the tight-binding approximation is well used in our system. Under the tight-binding approximation, the spin-orbit-coupled BECs in deep optical lattices can be described by two coupled discrete nonlinear Schrödinger equations [15]:

$$\begin{aligned} i\frac{d\psi_{\uparrow,n}}{dt} &= -\Gamma(\psi_{\uparrow,n+1} + \psi_{\uparrow,n-1}) + i\frac{\chi}{2}(\psi_{\downarrow,n+1} - \psi_{\downarrow,n-1}) \\ &\quad + \Omega\psi_{\uparrow,n} + (g|\psi_{\uparrow,n}|^2 + g_{12}|\psi_{\downarrow,n}|^2)\psi_{\uparrow,n}, \\ i\frac{d\psi_{\downarrow,n}}{dt} &= -\Gamma(\psi_{\downarrow,n+1} + \psi_{\downarrow,n-1}) + i\frac{\chi}{2}(\psi_{\uparrow,n+1} - \psi_{\uparrow,n-1}) \\ &\quad - \Omega\psi_{\downarrow,n} + (g_{12}|\psi_{\uparrow,n}|^2 + g|\psi_{\downarrow,n}|^2)\psi_{\downarrow,n}, \end{aligned} \quad (5)$$

where

$$\Gamma = \Gamma_{n,n+1} = \int \omega^*(x-n)\frac{\partial^2}{\partial x^2}\omega(x-n-1)dx, \quad (6)$$

$$g_{12} = \tilde{g}_{\uparrow\downarrow} \int |\omega(x-n)|^4 dx, \quad g = \tilde{g} \int |\omega(x-n)|^4 dx, \quad (7)$$

$$\chi \equiv \chi_{n,n+1} = 2\tilde{\chi} \int \omega^*(x-n)\frac{\partial}{\partial x}\omega(x-n-1)dx, \quad (8)$$

where $\omega(x-n)$ is the Wannier wave function, Γ is the dimensionless tunneling coefficient, and χ denotes the dimensionless SOC strength. Then the Hamilton of the system can be reduced to

$$\begin{aligned} H &= \sum_n \left\{ -\Gamma(\psi_{\uparrow,n}^*\psi_{\uparrow,n+1} + \psi_{\downarrow,n}^*\psi_{\downarrow,n+1}) \right. \\ &\quad \left. + i\frac{\chi}{2}\psi_{\uparrow,n}^*(\psi_{\downarrow,n+1} - \psi_{\downarrow,n-1}) + \frac{\Omega}{2}(|\psi_{\uparrow,n}|^2 - |\psi_{\downarrow,n}|^2) \right\} \\ &\quad + \text{c.c.} \\ &\quad + \sum_n \left\{ \frac{1}{2}(g|\psi_{\uparrow,n}|^4 + g|\psi_{\downarrow,n}|^4) + g_{12}|\psi_{\uparrow,n}|^2|\psi_{\downarrow,n}|^2 \right\}, \end{aligned} \quad (9)$$

where c.c. is the complex conjugate of the expression in the curly brackets of Eq. (9).

Because the central density of the localized state has a nearly Gaussian shape, it is good to use the Gaussian trial wave function to study the dynamical properties of spin-orbit-coupled BECs in deep optical lattices. We use the trial function [16,36]

$$\begin{aligned} \Psi(n, t) &= \begin{pmatrix} \psi_{\uparrow} \\ \psi_{\downarrow} \end{pmatrix} = \frac{e^{-\frac{(n-\xi)^2}{2R^2} + ip(n-\xi) + i\eta\frac{(n-\xi)^2}{2}}}{(2\sqrt{\pi}R)^{1/2}} \\ &\quad \times \begin{pmatrix} e^{i\frac{\phi}{2}}(\sqrt{1+s}) \\ -e^{-i\frac{\phi}{2}}(\sqrt{1-s}) \end{pmatrix}, \end{aligned} \quad (10)$$

where $R(t)$ and $\xi(t)$ represent the center-of-mass position and the width of the wave packet, respectively. $p(t)$ and $\eta(t)$ are

the related momenta and the variety rates of the width, respectively. $s(t)$ ($-1 < s < 1$) is the spin population difference between two pseudospin components i.e., the spin polarization $\langle\sigma_z\rangle = s$. And $\phi(t)$ is the phase difference between two pseudospin components. By inserting the trial wave function (10) into Eq. (9), we can get

$$\begin{aligned} H &= e^{-\gamma}(-2\Gamma \cos p + \chi \cos \phi \sqrt{1-s^2} \sin p) \\ &\quad + \frac{G_1 + G_2 s^2}{4\sqrt{2\pi}R} + \Omega s, \end{aligned} \quad (11)$$

where $G_1 = g + g_{12}$, $G_2 = g - g_{12}$, and $\gamma = \frac{R^4\eta^2+1}{4R^2}$. The Lagrangian density is

$$L = \sum_n \frac{i}{2}(\dot{\Psi}_n \Psi_n^* - \Psi_n^* \dot{\Psi}_n) - H,$$

where the dot means the derivative with respect to t . Inserting Eq. (10) into the Lagrangian density, we can get

$$\begin{aligned} L &= e^{-\gamma}(2\Gamma \cos p - \chi \cos \phi \sqrt{1-s^2} \sin p) \\ &\quad - \frac{1}{4}R^2\dot{\eta} + p\dot{\xi} - \frac{1}{2}s(2\Omega + \dot{\phi}) + \frac{G_1 + G_2 s^2}{4\sqrt{2\pi}R}. \end{aligned} \quad (12)$$

Solving the Euler-Lagrangian equations $\frac{d}{dt}\frac{\partial}{\partial q_i} = \frac{\partial L}{\partial q_i}$, ($q_i = \xi, p, R, \eta, \phi, s$), we can obtain the differential equations of motion:

$$\dot{p} = 0, \quad (13a)$$

$$\dot{R} = R\eta e^{-\gamma}(2\Gamma \sin p - \chi \sqrt{1-s^2} \cos \phi \sin p), \quad (13b)$$

$$\dot{\xi} = e^{-\gamma}(2\Gamma \sin p + \chi \sqrt{1-s^2} \cos \phi \cos p), \quad (13c)$$

$$\begin{aligned} \dot{\eta} &= e^{-\gamma} \left(\frac{R^4\eta^2 + 1}{R^4} - 2\eta^2 \right) (2\Gamma \cos p - \chi \cos \phi \sqrt{1-s^2} \sin p) \\ &\quad + \frac{G_1 + G_2 s^2}{2\sqrt{2\pi}R^3}, \end{aligned} \quad (13d)$$

$$\dot{\phi} = -2\Omega - \frac{G_2 s}{\sqrt{2\pi}R} + \frac{2\chi s e^{-\gamma} \cos \phi \sin p}{\sqrt{1-s^2}}, \quad (13e)$$

$$\dot{s} = -2e^{-\gamma} \chi \sqrt{1-s^2} \sin \phi \sin p. \quad (13f)$$

Equation (13a) indicates that the initial momentum of the wave packet remains unchanged in the process of dynamical evolution. Equation (13b) shows that the variation of the wave packet width depends on the time. $\dot{\xi}$ is the group velocity of the wave packet. Equations (13b), (13c), and (13d) simply show the dynamics of the wave packet. Then Eqs. (13e) and (13f) characterize, respectively, the change in the phase difference and the spin population difference between two pseudospin components of the spin-orbit-coupled BECs in deep optical lattices during the dynamical evolution. That is, the spin dynamics of the system is described by the internal Josephson equations (13e) and (13f). In the following, we will discuss the dynamics of the spin-orbit-coupled BECs loaded in a deep optical lattice.

III. THE LOCALIZED STATES WITHOUT SPIN EXCHANGE

Based on the variational equations, here we discuss in detail the transition of the localized states, including diffusion, self-trapping, breathers, and solitons. The derivative of the Hamilton (11) with respect to p is the group velocity v_g , which is the same as Eq. (13c), i.e., $\dot{\xi} = v_g = e^{-\gamma}(2\Gamma \sin p + \chi\sqrt{1-s^2} \cos \phi \cos p)$. Then the second order derivative of the Hamilton (11) with respect to p is the reciprocal of the effective mass,

$$\frac{1}{m^*} = \frac{\partial^2 H}{\partial p^2} = e^{-\gamma}(2\Gamma \cos p - \chi\sqrt{1-s^2} \cos \phi \sin p), \quad (14)$$

so the group velocity can be rewritten as

$$v_g = \frac{2\Gamma \tan p - \chi\sqrt{1-s^2} \cos \phi}{m^*(2\Gamma - \chi\sqrt{1-s^2} \cos \phi \tan p)}. \quad (15)$$

In the case of effective mass $m^* > 0$, i.e., $(2\Gamma \cos p - \chi\sqrt{1-s^2} \cos \phi \sin p) > 0$, the self-trapping will happen in this case when group velocity v_g tends to zero, i.e., $m^* \rightarrow \infty$. Diffusion can also be observed in this case. But there is no solitonic solution when the effective mass is positive. However, it is possible to form the bright soliton with a negative effective mass, i.e., $(2\Gamma \cos p - \chi\sqrt{1-s^2} \cos \phi \sin p) < 0$. With this condition, we can obtain a breather state near the soliton state. And with certain system parameters, there would be rich localized phenomena in the spin-orbit-coupled BECs loaded into deep optical lattices. Now we discuss in detail the localized states under different conditions.

For convenience, we first consider the case that the phase difference ϕ and spin population difference s between two pseudospin components remain unchanged over time, i.e., $\dot{\phi} = 0$, $\dot{s} = 0$. That leads to $s = s_0$ and $\phi = n\pi$; then we consider the case of $\phi = \pi$ in the following text. As shown in Eq. (13a), the momentum of the wave packet remains the initial value p_0 . We suppose the initial value of the change rate of the wave packet width $\eta_0 = 0$. Then the initial value of the Hamiltonian given by Eq. (11) is $H = e^{-\frac{1}{4R_0^2}}(-2\Gamma \cos p_0 - \chi\sqrt{1-s_0^2} \sin p_0) + \frac{G_1+G_2s_0^2}{4\sqrt{2\pi}R_0} + \Omega s_0$ since the Hamilton is a conserved quantity; that is, $H = H_0$ should be satisfied in the dynamical process.

For the self-trapping state, when $t \rightarrow \infty$, $R \rightarrow R_{\max}$, and $\eta \rightarrow \infty$, we have $\gamma = \frac{R^4\eta^2+1}{4R^2} \rightarrow \infty$, so from Eq. (13c), we can get $\dot{\xi} \rightarrow 0$. Using Eq. (11) we can get $H \rightarrow \Omega s_0 + \frac{G_1+G_2s_0^2}{4\sqrt{2\pi}R_{\max}} > 0$. Based on the conservation of energy $H = H_0$, the maximum value of the width of the wave packet is

$$R_{\max} = \frac{G_1 + G_2s_0^2}{4\sqrt{2\pi}(H_0 - \Omega s_0)}. \quad (16)$$

If self-trapping occurs, after a short expansion in the initial period, the width of the wave packet remains the maximum value over time, and the group velocity of the wave packet tends to zero.

We consider the case of $\dot{\phi} = 0$; by using Eq. (13e) we get $\Omega = \frac{G_1+G_2s_0}{4\sqrt{2\pi}R_{\max}}$. From Eq. (16) we can obtain

$$\Omega = \Omega_c = \frac{2e^{-\frac{1}{4R_0^2}}\alpha G_2s_0}{G_1 + G_2s_0^2} + \frac{G_2s_0}{2\sqrt{2\pi}R_0}. \quad (17)$$

In the case of the positive effective mass, the diffusion will appear when the wave packet diverges. In other words, when $(2\Gamma \cos p + \chi\sqrt{1-s^2} \sin p) > 0$, if the width of the wave packet tends to be infinity with time, for $t \rightarrow \infty$, we have $R \rightarrow \infty$, $\eta \rightarrow \infty$, so $\gamma = \frac{R^4\eta^2+1}{4R^2} \rightarrow 0$. Then from Eqs. (11) and (13c) we can get $H \rightarrow -(2\Gamma \cos p_0 + \chi \sin p_0\sqrt{1-s_0^2} - \Omega s_0)$ and $\dot{\xi} \rightarrow 2\Gamma \sin p_0 - \chi\sqrt{1-s_0^2} \cos p_0 \neq 0$. In this case, the center-of-mass position changes with time, and the wave packet keeps spreading. For convenience, we set $\alpha = 2\Gamma \cos p_0 + \chi \sin p_0\sqrt{1-s_0^2}$. We assume $\Omega > 0$, and when $\Omega s_0 < \alpha$, $H \rightarrow -(\alpha - \Omega s_0) < 0$.

Hence, the transition critical condition between self-trapping and diffusion can be obtained by $H_0 = 0$. Combining Eqs. (11), (16), and (17), the critical condition now can be written as

$$F_1 = \frac{2\alpha G_2s_0^2}{G_1 + G_2s_0^2} + \frac{G_1 + 3G_2s_0^2}{4e^{-\frac{1}{4R_0^2}}\sqrt{2\pi}R_0} - \alpha = 0. \quad (18)$$

If F_1 is positive, the wave packet stops expanding near the initial position; that is, self-trapping occurs. By contrast, the width of the wave packet tends to infinity in the regime of diffusion with negative F_1 .

Different from the case with positive effective mass, we can observe not only diffusion and self-trapping but also breathers and solitons when the effective mass is negative. In other words, when $m^* < 0$, i.e., $\alpha < 0$, the localized phenomenon is richer. Similar to the case of $m^* > 0$, for $t \rightarrow \infty$, $R \rightarrow \infty$, and $\eta \rightarrow 0$, we obtain $\dot{\xi} \rightarrow 2\Gamma \sin p_0 - \chi\sqrt{1-s_0^2} \cos p_0$ and $H \rightarrow -(\alpha - \Omega s_0) > 0$ in the diffusion region. The region of self-trapping, i.e., $R \rightarrow R_{\max}$, $\dot{\xi} \rightarrow 0$ as $t \rightarrow \infty$, is given by $H_0 > |\alpha - \Omega s_0|$. Equation (11) leads the critical condition of the transition between diffusion and self-trapping as

$$F_2 = \frac{G_1 + G_2s_0^2}{4\sqrt{2\pi}R_0} + (1 - e^{-\frac{1}{4R_0^2}})\alpha = 0. \quad (19)$$

For $F_2 > 0$, the self-trapping state occurs, and the diffusion state occurs when $F_2 < 0$.

Beyond that, it is possible to find the soliton solution with a negative effective mass. The wave packet does not expand, and the group velocity remains the initial value over time when the soliton appears, i.e., $\dot{R} = 0$, $\dot{\eta} = 0$, $\dot{\xi} = \text{const}$ for $t \rightarrow \infty$. For Eq. (13b) and $\dot{R} = 0$ we have $\eta = 0$. The same as in the case with $m^* > 0$, using $\dot{\phi} = 0$, now Ω has the following form:

$$\Omega = \Omega_{\text{sol}} = -\frac{G_2s_0}{2\sqrt{2\pi}R_0} - \frac{s_0e^{-\frac{1}{4R_0^2}}\chi \sin p_0}{\sqrt{1-s_0^2}}. \quad (20)$$

According to $\dot{R} = 0$ [Eq. (13b)], $\dot{\eta} = 0$ [Eq. (13d)], and Eq. (20), we have the critical condition of the soliton

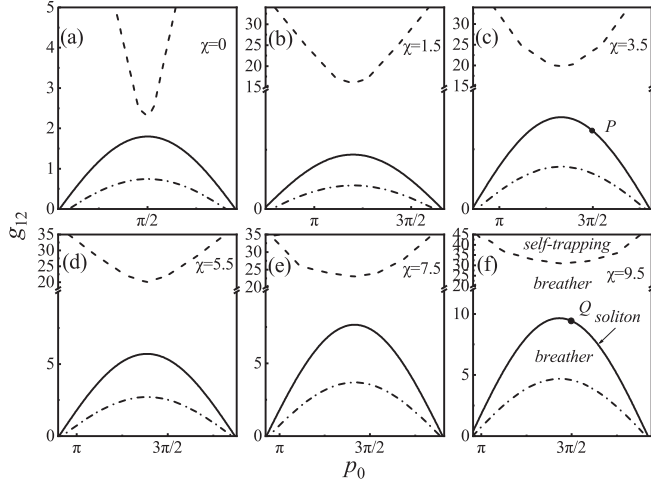


FIG. 1. The dynamics phase diagram in the (p_0, g_{12}) plane with different χ . The dashed lines obtained numerically show the boundary between self-trapping and the breather. The dash-dotted lines are used to separate the self-trapped and diffusive regions. The solid lines represent the solitonic solution. The other parameters are $R_0 = 5$, $g = 0.3$, $s_0 = 0.25$.

state:

$$F_3 = \frac{e^{-\frac{1}{4k_0^4}}}{R_0^4} \alpha + \frac{G_1 + G_2 s_0^2}{2\sqrt{2\pi} R_0^3} = 0. \quad (21)$$

When Eq. (21) is satisfied, the center-of-mass position of the wave packet moves with constant group velocity, and the shape of the wave packet does not change with time. In the region between $F_2 > 0$ and $F_3 < 0$ or the region with $F_3 > 0$, a breather occurs with an oscillating width of the wave packet and invariant group velocity. That is, a soliton or breather state occurs. In this case, Eq. (20) guarantees that the spin dynamics of the system is inhibited and the spin polarization remains

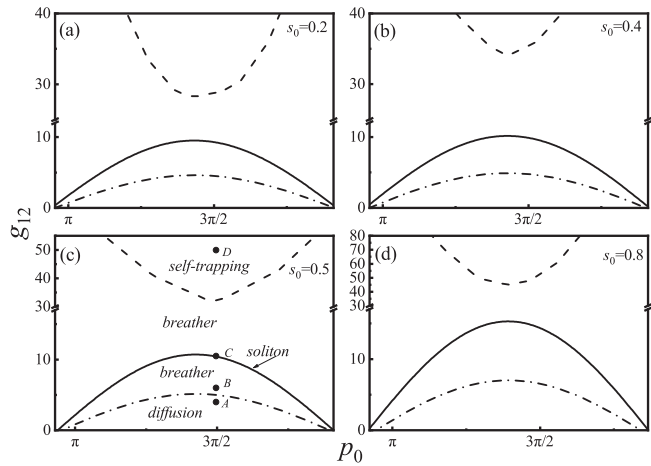


FIG. 2. The dynamics phase diagram in the (p_0, g_{12}) plane with different s_0 . The dashed lines obtained numerically show the boundary between self-trapping and the breather. The dash-dotted lines are used to separate the self-trapped and diffusive regions. The solid lines represent the solitonic solution. The other parameters are $R_0 = 5$, $g = 0.3$, $\chi = 9.5$.

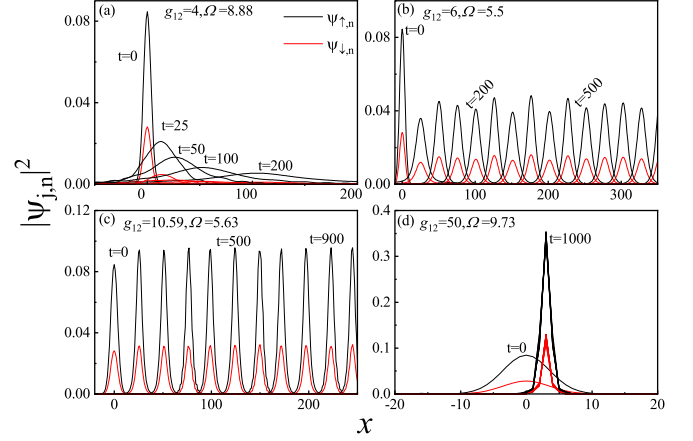


FIG. 3. Numerical simulation results for the time evolution of the wave packet profiles of points A, B, C, and D marked in Fig. 2(c). The black and red (gray) lines illustrate the pseudospin components ψ_{\uparrow} and ψ_{\downarrow} , respectively.

$s = s_0$. We analytically characterize the transition between the localized phenomena under different conditions. These results show that the dynamics of the spin-orbit-coupled BECs in deep optical lattices are strongly influenced by the atomic interaction, SOC strength, and Raman detuning. According to the critical conditions provided by Eqs. (17)–(21) for the occurring diffusion, self-trapping, soliton, and breather in different cases, we can easily derive the dynamical phase diagram.

The dynamical phase diagrams in the plane (p_0, g_{12}) are shown in Figs. 1 and 2. As we discussed, the phase diagram is richer in the case with $m^* < 0$. We are primarily interested in the phase diagram when the effective mass is negative. For different strengths of SOC, the inter-species interaction g_{12} versus momentum p_0 is illustrated in Fig. 1 with $s_0 = 0.25$, $R_0 = 5$, and $g = 0.3$. The parameter space of the system is divided into four regions. The solid lines depict the soliton solutions; the dash-dotted curves are the regions of

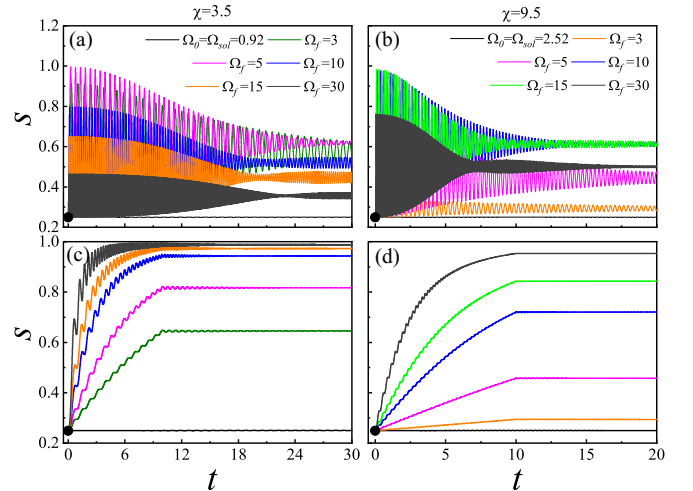


FIG. 4. Time evolution of the spin polarizations for sudden (top) and linear (bottom) quenches of Ω from $\Omega_0 = \Omega_{\text{sol}}$ to different Ω_f . $R_0 = 5$, $g = 0.3$, $s_0 = 0.25$, $p_0 = 3\pi/2$. $\chi = 3.5$ and $g_{12} = 3.29$ in the left column, and $\chi = 9.5$ and $g_{12} = 9.44$ in the right column.

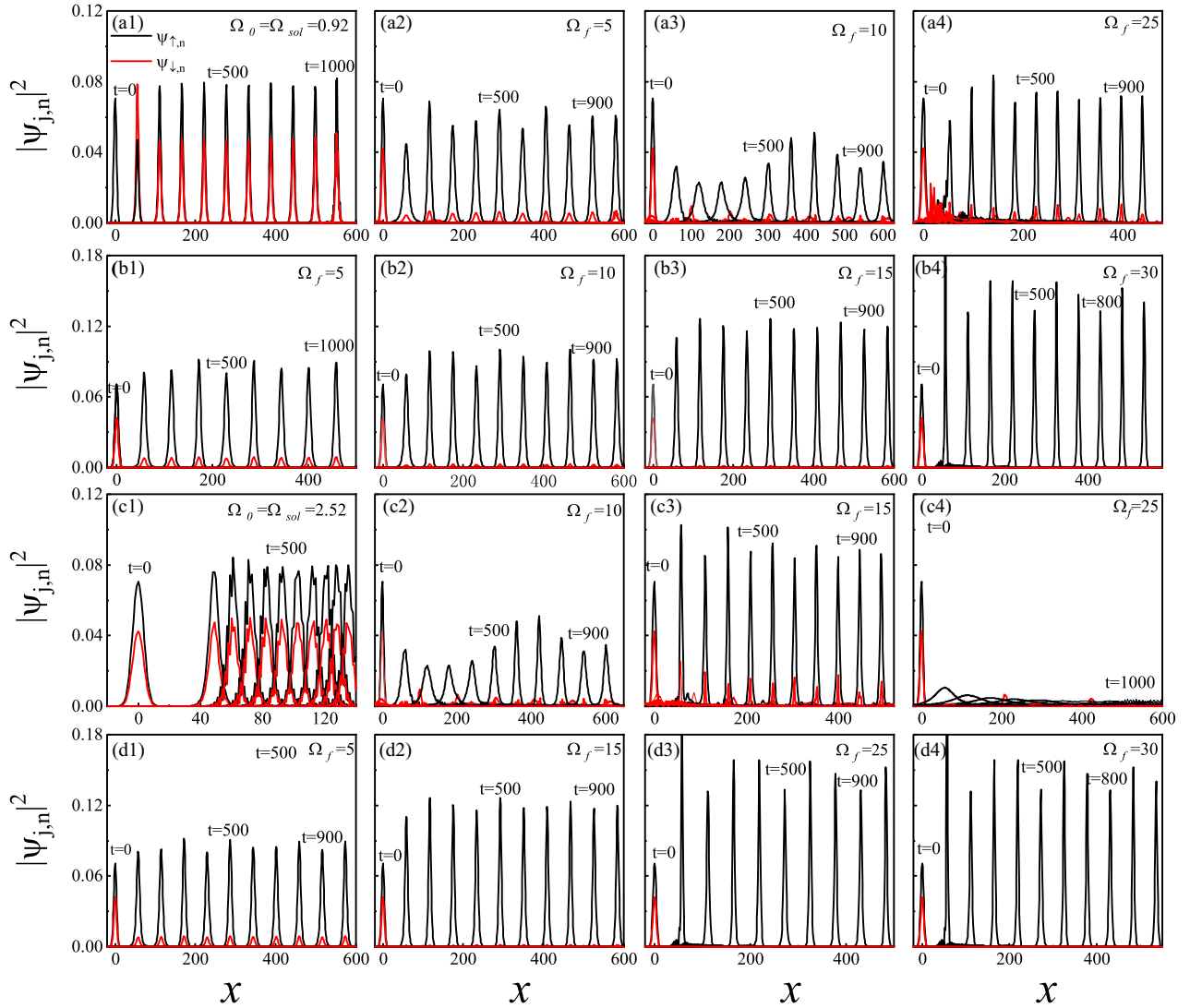


FIG. 5. Numerical simulation results for the time evolution of wave packet profiles. The black and red (gray) lines illustrate pseudospin components ψ_\uparrow and ψ_\downarrow , respectively. $R_0 = 5$, $g = 0.3$, $s_0 = 0.25$, and $p_0 = 3\pi/2$. (a1)–(a4) For point P ($\chi = 3.5$) as marked in Fig. 1(c) when suddenly quenching the Raman detuning from Ω_0 to different Ω_f and (b1)–(b4) the corresponding linear quenching of the Raman detuning from Ω_0 to different Ω_f . (c1)–(c4) For point Q ($\chi = 9.5$) as marked in Fig. 1(f) when suddenly quenching the Raman detuning from Ω_0 to different Ω_f and (d1)–(d4) the corresponding linear quenching of the Raman detuning from Ω_0 to different Ω_f .

diffusion. On both sides of the solid lines are the regions for the breather state. The dashed lines distinguish the regions of self-trapping and breather phenomena. Note that the dashed lines are given by numerical simulations. With the increasing of the SOC strength, the regions for diffusion and breather states expand. And the appearance of self-trapping requires larger interspecies interaction.

Phase diagrams with different spin population differences s_0 are shown in Fig. 2. The other parameters are the same as in Fig. 1 except $\chi = 9.5$. The dashed lines which distinguish breather and self-trapping states are obtained numerically. Figure 2 shows that with the increase of s_0 , the regions for the diffusion and breather become larger. The formation of solitons and self-trapping needs larger interspecies interaction.

We analytically show the dynamical evolution in the phase diagram with fixed s_0 and fixed χ in Figs. 1 and 2, respec-

tively. To confirm our analytical results, we choose points A, B, C, and D in Fig. 2(c) and numerically simulate the localized states by the fourth-order Runge-Kutta method. The results of direct numerical simulations of Eq. (5) with parameters as marked by A, B, C, and D in Fig. 2(c) are shown in Fig. 3. In Fig. 3, the red (gray) lines and the black lines denote two pseudospin components. As expected, the diffusion, breather, soliton, and self-trapping occur one after another as the interspecies interaction increases. Figure 3 confirms our analytical prediction.

IV. THE LOCALIZED STATES WITH SPIN EXCHANGE

In the above, we considered the case of $\dot{s} = 0$, in which atoms between two pseudospin components do not exchange. When Eqs. (17) and (20) are satisfied, we obtain the critical condition for the transition of localized states, and the time

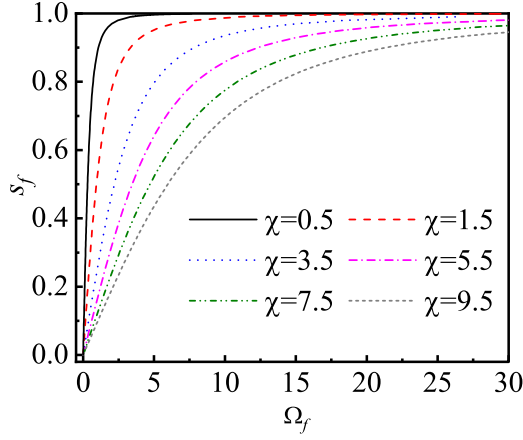


FIG. 6. The variation of polarization s_f against Ω_f for different values of χ . $R_0 = 5$, $g = 0.3$, and $p_0 = 3\pi/2$.

evolution of these localized states is illustrated in Fig. 3. In this case the spin dynamics is inhibited, and the system is in a fixed polarization $\langle \sigma_z \rangle = s_0$. Now we consider the case with $\dot{s} \neq 0$, in which the spin dynamics is excited. Here, we focus on discussing the excitation of the spin dynamics upon soliton states via quenching the Raman detuning from $\Omega_0 = \Omega_{\text{sol}}$ given by Eq. (20) to a final Raman detuning strength Ω_f by numerical simulation of Eq. (5). Because $\Omega_f \neq \Omega_{\text{sol}}$, the condition (20) is not satisfied, i.e., $\dot{s} \neq 0$; then the spin dynamics will be excited. Correspondingly, the polarization and the soliton dynamics of the system will be modified. We use two quenching methods, i.e., sudden and linear quenchings of Raman detuning, to discuss the spin dynamics, phase transition, and wave packet dynamics by numerical simulation of Eq. (5). Interestingly, we find that the linear quenching of Raman detuning Ω can induce a controllable phase transition from the unpolarized phase to an expected polarized phase, while the soliton or breather dynamics is maintained.

A. Spin dynamics excited by sudden quenching of Ω

Without loss of generality, we consider the cases of soliton states as marked by points P and Q in Figs. 1(c) and 1(f), respectively. If $\Omega = \Omega_{\text{sol}}$, the soliton states occur [see Figs. 5(a1) and 5(c1)], and as depicted by the black lines in Figs. 4(a) and 4(b), atoms in the two pseudospin components do not exchange ($s = s_0$). Taking other system parameters to be the same as in Figs. 1(c) and 1(f) except Ω and quenching the value of Raman detuning Ω from $\Omega_0 = \Omega_{\text{sol}}$ to different Ω_f suddenly, Figs. 4(a) and 4(b) show the spin dynamic of the system with different Ω_f for points P and Q , respectively. The corresponding wave packet dynamics with different Ω_f for points P and Q are illustrated in Figs. 5(a2)–5(a4) and 5(c2)–5(c4), respectively. Figures 4(a) and 4(b) show that if $\Omega \neq \Omega_{\text{sol}}$, atoms between two pseudospin components exchange ($s \neq s_0$), and the exchange of atoms between two pseudospin components takes the form of damped oscillations, the spin dynamics is excited. Finally, the system is changed to a new polarized state with $s = \bar{s} \neq s_0$. When $\Omega_f > \Omega_{\text{sol}}$ and as the Raman detuning Ω_f increases, the amplitude of the damped

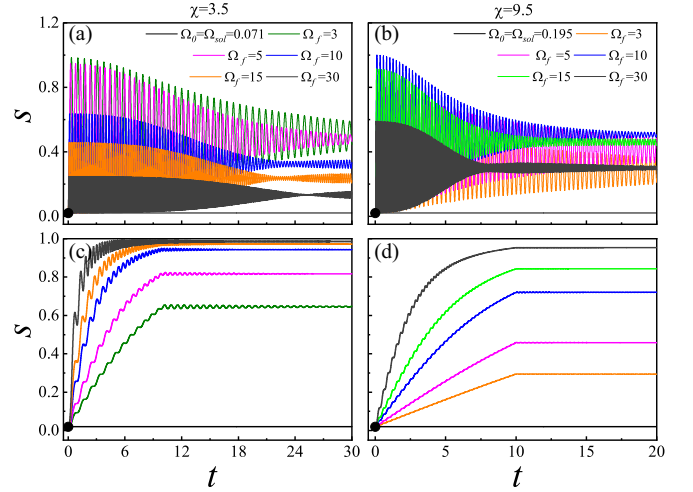


FIG. 7. Time evolution of the spin polarization for sudden (top) and linear (bottom) quenchings of Ω from $\Omega_0 = \Omega_{\text{sol}}$ to different Ω_f . $R_0 = 5$, $g = 0.3$, $s_0 = 0.02$, $p_0 = 3\pi/2$. $\chi = 3.5$ and $g_{12} = 3.2$ in the left column, and $\chi = 9.5$ and $g_{12} = 9.15$ in the right column.

oscillations of s also increases, and the damped oscillations also last longer, which is more obvious for small SOC strength [Fig. 4(a)]. The new polarized states are characterized by $\bar{s} > s_0$. The value of \bar{s} is not controllable. That is, to have a highly polarized state via sudden quenching Ω cannot realize a controllable polarized state with an expected s . Figures 4(a) and 4(b) also illustrate that the period of the spin exchange is decreased by increasing SOC strength χ and Raman detuning Ω , and the spin dynamics of the quenching system is enhanced by SOC. Sudden quenching of Ω results in the transition between different polarized states, that is, a highly polarized state (larger s) is realized. The corresponding time evolution of wave packets with different Ω_f is shown in Figs. 5(a2)–5(a4) for $\chi = 3.5$ and Figs. 5(c2)–5(c4) for $\chi = 9.5$. The results of the numerical simulation show that for weak Ω_f , the quasisoliton or breather states can exist even though $\Omega_f \neq \Omega_{\text{sol}}$, especially for small SOC strength χ [Figs. 5(a2)–5(a4)]. However, we can see that the soliton or breather state finally trends toward the diffusion state for larger χ and Ω_f [Fig. 5(c4)]. That is, for sudden quenching of Ω , the soliton or breather state will be unstable when Ω_f is larger, especially for larger χ .

B. Spin dynamics excited by linear quenching of Ω

If we quench Raman detuning Ω from $\Omega_0 = \Omega_{\text{sol}}$ to Ω_f sufficiently slowly, we expect the soliton or breather states of the system can be maintained. If this is true, Eqs. (20) and (21) should hold. Because the system parameters, i.e., atomic interactions g and g_{12} , SOC strength χ , momentum p_0 , and wave packet radius R_0 , are fixed, when Raman detuning Ω is slowly quenched from Ω_{sol} to Ω_f , Eq. (20) indicates that a new polarized state with spin polarization $s = s_f$ can be obtained. That is, a controllable polarized state with expected polarization s_f can be realized by slowly quenching Ω . For given parameters g , χ , p_0 , and R_0 , Eqs. (20) and (21) determine the relationship of s_f and $\Omega = \Omega_f$. The variation of

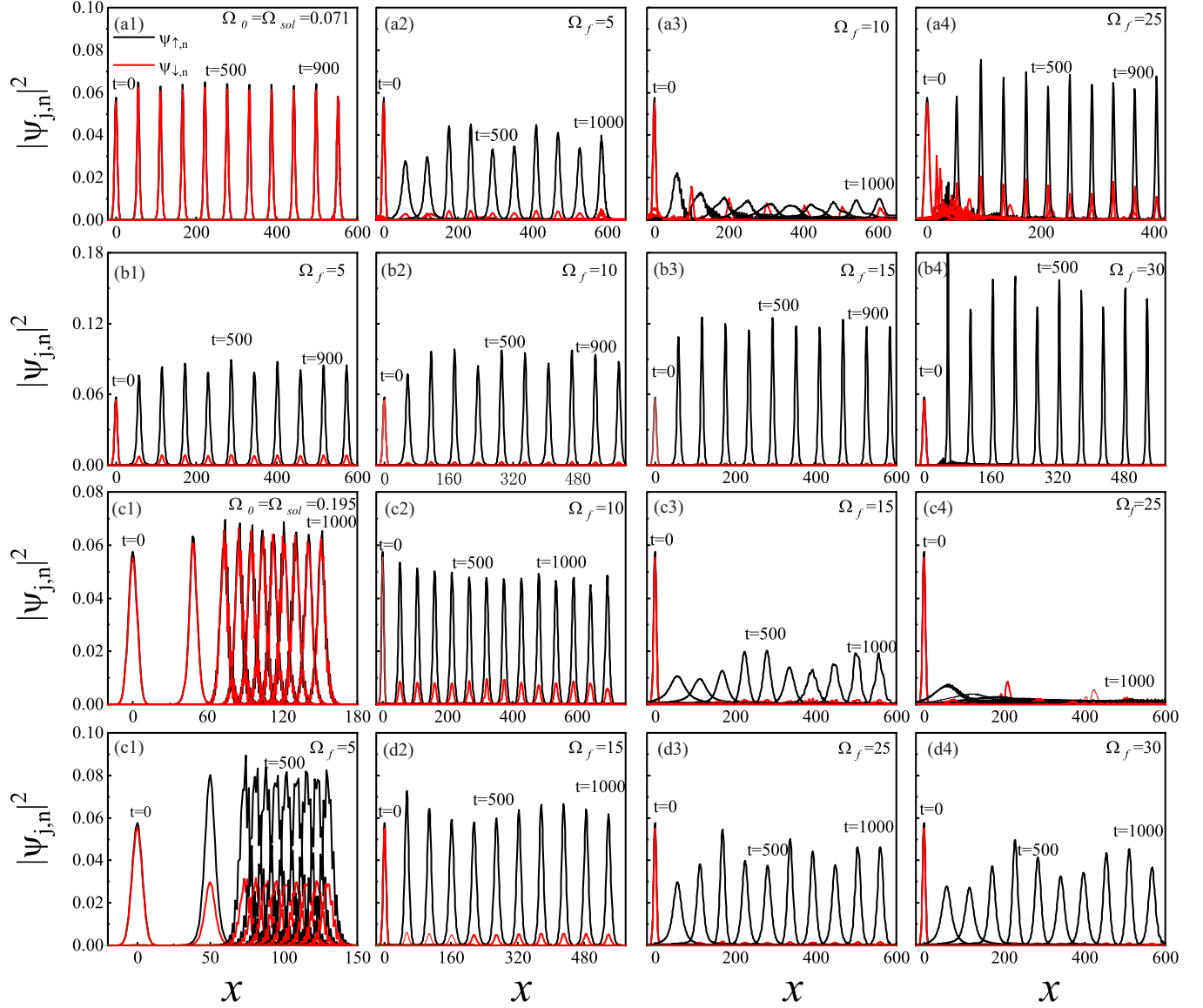


FIG. 8. Numerical simulation results for the time evolution of the wave packet profiles. The black and red (gray) lines illustrate pseudospin components ψ_{\uparrow} and ψ_{\downarrow} , respectively. $R_0 = 5$, $g = 0.3$, $s_0 = 0.02$, and $p_0 = 3\pi/2$. (a1)–(a4) For $\chi = 3.5$ when suddenly quenching the Raman detuning from Ω_0 to different Ω_f and (b1)–(b4) the corresponding linear quenching of the Raman detuning from Ω_0 to different Ω_f . (c1)–(c4) For $\chi = 9.5$ when suddenly quenching the Raman detuning from Ω_0 to different Ω_f and (d1)–(d4) the corresponding linear quenching of the Raman detuning from Ω_0 to different Ω_f .

s_f versus Ω_f is shown in Fig. 6 for different χ . For fixed χ , s_f increases with Raman detuning Ω . That is, a higher polarized state can be realized with a larger Ω_f , and for a sufficiently large Ω_f , a fully polarized state with $s_f \rightarrow 1$ can be realized. The smaller the SOC strength χ is, the easier the fully polarized state is to realize (with small Ω_f). Here, we use a linear quenching of Raman detuning formulated as

$$\Omega(t) = \begin{cases} \frac{\Omega_f - \Omega_0}{\tau_q} + \Omega_0 & 0 \leq t \leq \tau_q, \\ \Omega_f & t > \tau_q, \end{cases} \quad (22)$$

where $\Omega_0 = \Omega_{\text{sol}}$ is given by Eq. (20), Ω_f is the quenched final Raman detuning, and τ_q is the quenching time. Numerical simulations show that when $\tau_q \geq 5$, a controllable spin polarization transition can be realized. Figures 4(c) and 4(d) show

the time variation of polarization s via linear quenching of Raman detuning Ω with $\tau_q = 10$ for the cases with $\chi = 3.5$ and $\chi = 9.5$, respectively, which correspond to the cases with sudden quenching of Ω shown in Figs. 4(a) and 4(b), respectively. We find that, for a given Ω_f , the polarization s is manipulated from $s_0 = 0.25$ to a final polarization $s = s_f$ given by Eq. (20) (see Fig. 6). For given values of χ and Ω_f , the final values of s obtained from numerical simulations shown in Figs. 4(c) and 4(d) agree with the theoretical results shown in Fig. 6. That is, a controllable polarization transition is achieved. Figures 4(c) and 4(d) also illustrate that, different from the case of sudden quenching of Ω , the linear quenching of Ω results in nearly smothering the transition of spin polarization, especially for larger SOC strength χ . Figures 5(b1)–5(b4) and 5(d1)–5(d4) show the corresponding time evolution of the wave packets

via linear quenching of Raman detuning Ω . Interestingly, the soliton or breather state is maintained for all values of Ω_f .

To further confirm the reasonableness of the linear quenching of Raman detuning Ω , Figs. 7 and 8 show the results of quenching Raman detuning Ω from an unpolarized state with $s_0 \rightarrow 0$ to a polarized state. Both sudden and linear quenching results are shown. The results are similar to the case with $s_0 = 0.25$ (Figs. 4 and 5); that is, the linear quenching of Raman detuning Ω realizes the controllable polarization transition and maintains the soliton or breather dynamics of the system, while the sudden quenching of Ω does not. Particularly, a controllable phase transition from an unpolarized state ($s_0 \rightarrow 0$) to an expected polarized state $s = s_f$ is realized.

V. CONCLUSION

In conclusion, we have investigated localization of two-component BECs with SOC trapped in deep optical lattices based on the variational method and numerical simulation. Rich localized states in the system, such as diffusion, self-trapping, soliton, and breather states, were observed. For all of these localized phenomena, the transition critical conditions among these states were derived analytically. Correspondingly, a detailed dynamical phase diagram describing the different dynamical regimes was derived. The results suggest that the atomic interaction, SOC strength, and Raman

detuning play key roles in the localization of the system. The localization phenomenon both with (when Raman detuning satisfies a critical condition) and without (when Raman detuning does not satisfy the critical condition) spin dynamics was discussed. In addition, the spin dynamics excited upon the soliton or breather state via quenching of Raman detuning was discussed. Sudden quenching of Raman detuning results in a transition among different polarized states, but the soliton or breather states finally change. Particularly, linear quenching of Raman detuning can realize a controllable phase transition while the soliton or breather state is maintained. Our results provide theoretical evidence for experimental observation of rich localized states of spin-orbit-coupled BECs in optical lattices. Beyond that, these results further illustrate that spin-orbit-coupled BECs render a new test bed with a well-controlled feature for manipulating nonlinear matter waves and exploring dynamic quantum phase transitions in ultracold atom systems.

ACKNOWLEDGMENTS

This work is supported by the National Natural Science Foundation of China under Grants No. 12164042, No. 11764039, No. 11847304, and No. 11865014, by the Natural Science Foundation of Gansu Province under Grant No. 17JR5RA076, and by the Scientific Research Project of Gansu Higher Education under Grant No. 2016A-005.

-
- [1] D. Xiao, M.-C. Chang, and Q. Niu, *Rev. Mod. Phys.* **82**, 1959 (2010).
 - [2] M. Z. Hasan and C. L. Kane, *Rev. Mod. Phys.* **82**, 3045 (2010).
 - [3] T. Morimoto and A. Furusaki, *Phys. Rev. B* **89**, 035117 (2014).
 - [4] Y.-J. Lin, K. Jiménez-García, and I. B. Spielman, *Nature (London)* **471**, 83 (2011).
 - [5] J. Y. Zhang, S. C. Ji, Z. Chen, L. Zhang, Z. D. Du, B. Yan, G. S. Pan, B. Zhao, Y. J. Deng, H. Zhai, S. Chen, and J. W. Pan, *Phys. Rev. Lett.* **109**, 115301 (2012).
 - [6] C. Qu, C. Hamner, M. Gong, C. Zhang, and P. Engels, *Phys. Rev. A* **88**, 021604(R) (2013).
 - [7] L. Huang, Z. Meng, P. Wang, P. Peng, S. L. Zhang, L. Chen, D. Li, Q. Zhou, and J. Zhang, *Nat. Phys.* **12**, 540 (2016).
 - [8] Z. Wu, L. Zhang, W. Sun, X.-T. Xu, B.-Z. Wang, S.-C. Ji, Y. Deng, S. Chen, X.-J. Liu, and J.-W. Pan, *Science* **354**, 83 (2016).
 - [9] Z. Meng, L. Huang, P. Peng, D. Li, L. Chen, Y. Xu, C. Zhang, P. Wang, and J. Zhang, *Phys. Rev. Lett.* **117**, 235304 (2016).
 - [10] H. Zhai, *Rep. Prog. Phys.* **78**, 026001 (2015); R. A. Williams, M. C. Beeler, L. J. LeBlanc, K. Jimenez-Garcia, and I. B. Spielman, *Phys. Rev. Lett.* **111**, 095301 (2013).
 - [11] T.-L. Ho and S. Zhang, *Phys. Rev. Lett.* **107**, 150403 (2011).
 - [12] Y.-J. Lin, R. L. Compton, A. R. Perry, W. D. Phillips, J. V. Porto, and I. B. Spielman, *Phys. Rev. Lett.* **102**, 130401 (2009).
 - [13] Y.-J. Lin, R. L. Compton, K. Jimenez-Garcia, J. V. Porto, and I. B. Spielman, *Nature (London)* **462**, 628 (2009).
 - [14] J.-R. Li, J. Lee, W. Huang, S. Burchesky, B. Shteynas, F. Ç. Top, A. O. Jamison, and W. Ketterle, *Nature (London)* **543**, 91 (2017).
 - [15] M. Salerno, F. Kh. Abdullaev, A. Gammal, and L. Tomio, *Phys. Rev. A* **94**, 043602 (2016).
 - [16] Y.-C. Zhang, Y. Jian, Z.-F. Yu, A.-X. Zhang, and J.-K. Xue, *Phys. Rev. E* **102**, 032220 (2020); Z. Chen and H. Zhai, *Phys. Rev. A* **86**, 041604(R) (2012).
 - [17] C. H. Li, C. L. Qu, R. J. Niffenegger, S.-J. Wang, M. He, D. B. Blasing, A. J. Olson, C. H. Greene, Y. Lyanda-Geller, Q. Zhou, C. Zhang, and Y. P. Chen, *Nat. Commun.* **10**, 375 (2019).
 - [18] Y. A. Bychkov and E. I. Rashba, *J. Phys. C* **17**, 6039 (1984).
 - [19] G. Dresselhaus, *Phys. Rev.* **100**, 580 (1955).
 - [20] C. Hamner, Y. Zhang, M. A. Khamehchi, M. J. Davis, and P. Engels, *Phys. Rev. Lett.* **114**, 070401 (2015).
 - [21] V. Galitski and I. B. Spielman, *Nature (London)* **494**, 49 (2013).
 - [22] Y. Zhang, G. Chen, and C. Zhang, *Sci. Rep.* **3**, 1937 (2013).
 - [23] K. Jimenez-Garcia, L. J. LeBlanc, R. A. Williams, M. C. Beeler, C. Qu, M. Gong, C. Zhang, and I. B. Spielman, *Phys. Rev. Lett.* **114**, 125301 (2015).
 - [24] X. Luo, L. Wu, J. Chen, Q. Guan, K. Gao, Z. Xu, L. You, and R. Wang, *Sci. Rep.* **6**, 18983 (2016).
 - [25] H. Hu, B. Ramachandhran, H. Pu, and X.-J. Liu, *Phys. Rev. Lett.* **108**, 010402 (2012).
 - [26] Y. Li, L. P. Pitaevskii, and S. Stringari, *Phys. Rev. Lett.* **108**, 225301 (2012).
 - [27] Y. Li, G. I. Martone, L. P. Pitaevskii, and S. Stringari, *Phys. Rev. Lett.* **110**, 235302 (2013).
 - [28] C. Hamner, C. Qu, Y. Zhang, J. Chang, M. Gong, C. Zhang, and P. Engels, *Nat. Commun.* **5**, 4023 (2014).

- [29] W. Zheng, Z.-Q. Yu, X. Cui, and H. Zhai, *J. Phys. B* **46**, 134007 (2013).
- [30] M. A. Khamehchi, Y. Zhang, C. Hamner, T. Busch, and P. Engels, *Phys. Rev. A* **90**, 063624 (2014).
- [31] S.-C. Ji, L. Zhang, X.-T. Xu, Z. Wu, Y. Deng, S. Chen, and J.-W. Pan, *Phys. Rev. Lett.* **114**, 105301 (2015).
- [32] A. Trombettoni and A. Smerzi, *J. Phys. B* **34**, 4711 (2001).
- [33] M. Aidelsburger, M. Atala, S. Nascimbene, S. Trotzky, Y.-A. Chen, and I. Bloch, *Phys. Rev. Lett.* **107**, 255301 (2011).
- [34] H. Miyake, G. A. Siviloglou, C. J. Kennedy, W. C. Burton, and W. Ketterle, *Phys. Rev. Lett.* **111**, 185302 (2013).
- [35] C. J. Kennedy, W. C. Burton, W. C. Chung, and W. Ketterle, *Nat. Phys.* **11**, 859 (2015).
- [36] L. D. Carr, M. J. Holland, and B. A. Malomed, *J. Phys. B* **38**, 3217 (2005).
- [37] Z. Chen and B. A. Malomed, *Phys. Rev. E* **95**, 032217 (2017).
- [38] F. K. Abdullaev, A. Gammal, A. M. Kamchatnov, and L. Tomio, *Int. J. Mod. Phys. B* **19**, 3415 (2005).
- [39] M. J. Edmonds, J. Otterbach, R. G. Unanyan, M. Fleischhauer, M. Titov, and P. Öhberg, *New J. Phys.* **14**, 073056 (2012).
- [40] M. Bukov, L. D'Alessio, and A. Polkovnikov, *Adv. Phys.* **64**, 139 (2015).
- [41] S. Longhi, M. Marangoni, M. Lobino, R. Ramponi, P. Laporta, E. Cianci, and V. Foglietti, *Phys. Rev. Lett.* **96**, 243901 (2006).
- [42] R. Iyer, J. S. Aitchison, J. Wan, M. M. Dignam, and C. M. deSterke, *Opt. Express* **15**, 3212 (2007).
- [43] H. Lignier, C. Sias, D. Ciampini, Y. Singh, A. Zenesini, O. Morsch, and E. Arimondo, *Phys. Rev. Lett.* **99**, 220403 (2007).
- [44] E. Trias, J. J. Mazo, and T. P. Orlando, *Phys. Rev. Lett.* **84**, 741 (2000).
- [45] A. V. Ustinov, *Chaos* **13**, 716 (2003).
- [46] U. T. Schwarz, L. Q. English, and A. J. Sievers, *Phys. Rev. Lett.* **83**, 223 (1999).
- [47] M. Sato and A. J. Sievers, *Nature (London)* **432**, 486 (2004).
- [48] B. Eiermann, T. Anker, M. Albiez, M. Taglieber, P. Treutlein, K.-P. Marzlin, and M. K. Oberthaler, *Phys. Rev. Lett.* **92**, 230401 (2004).
- [49] A. Trombettoni and A. Smerzi, *Phys. Rev. Lett.* **86**, 2353 (2001).
- [50] O. Morsch, M. Cristiani, J. H. Muller, D. Ciampini, and E. Arimondo, *Phys. Rev. A* **66**, 021601(R) (2002).
- [51] T. J. Alexander, E. A. Ostrovskaya, and Y. S. Kivshar, *Phys. Rev. Lett.* **96**, 040401 (2006).
- [52] R. Hipolito and A. Polkovnikov, *Phys. Rev. A* **81**, 013621 (2010).
- [53] M. Albiez, R. Gati, J. Fölling, S. Hunsmann, M. Cristiani, and M. K. Oberthaler, *Phys. Rev. Lett.* **95**, 010402 (2005).
- [54] T. Anker, M. Albiez, R. Gati, S. Hunsmann, B. Eiermann, A. Trombettoni, and M. K. Oberthaler, *Phys. Rev. Lett.* **94**, 020403 (2005).
- [55] S. L. Cornish, S. T. Thompson, and C. E. Wieman, *Phys. Rev. Lett.* **96**, 170401 (2006).
- [56] S. Burger, K. Bongs, S. Dettmer, W. Ertmer, K. Sengstock, A. Sanpera, G. V. Shlyapnikov, and M. Lewenstein, *Phys. Rev. Lett.* **83**, 5198 (1999).
- [57] B. P. Anderson, P. C. Haljan, C. A. Regal, D. L. Feder, L. A. Collins, C. W. Clark, and E. A. Cornell, *Phys. Rev. Lett.* **86**, 2926 (2001).
- [58] S. Stellmer, C. Becker, P. Soltan-Panahi, E.-M. Richter, S. Dörscher, M. Baumert, J. Kronjäger, K. Bongs, and K. Sengstock, *Phys. Rev. Lett.* **101**, 120406 (2008).
- [59] D. L. Wang, X. H. Yan, and W. M. Liu, *Phys. Rev. E* **78**, 026606 (2008).
- [60] Z. X. Liang, Z. D. Zhang, and W. M. Liu, *Phys. Rev. Lett.* **94**, 050402 (2005).
- [61] Z. D. Li, P. B. He, L. Li, J. Q. Liang, and W. M. Liu, *Phys. Rev. A* **71**, 053611 (2005).
- [62] X. J. Jiang, Z. W. Fan, Z. P. Chen, W. Pang, Y. Y. Li, and B. A. Malomed, *Phys. Rev. A* **93**, 023633 (2016).
- [63] H. Sakaguchi and B. A. Malomed, *Phys. Rev. A* **97**, 013607 (2018).
- [64] V. A. Brazhnyi, V. V. Konotop, and L. P. Pitaevskii, *Phys. Rev. A* **73**, 053601 (2006).
- [65] C. Becker, S. Stellmer, P. Soltan-Panahi, S. Dörscher, M. Baumert, E.-M. Richter, J. Kronjäger, K. Bongs, and K. Sengstock, *Nat. Phys.* **4**, 496 (2008).
- [66] C. Hamner, J. J. Chang, P. Engels, and M. A. Hofer, *Phys. Rev. Lett.* **106**, 065302 (2011).
- [67] S. Middelkamp, J. J. Chang, C. Hamner, R. CarreteroGonzález, P. G. Kevrekidis, V. Achilleos, D. J. Frantzeskakis, P. Schmelcher, and P. Engels, *Phys. Lett. A* **375**, 642 (2011).
- [68] D. Yan, J. J. Chang, C. Hamner, P. G. Kevrekidis, P. Engels, V. Achilleos, D. J. Frantzeskakis, R. Carretero-González, and P. Schmelcher, *Phys. Rev. A* **84**, 053630 (2011).
- [69] S. Pandey, H. Mas, G. Drougakis, P. Thekkepatt, V. Bolpasi, G. Vasilakis, K. Poullos, and W. von Klitzing, *Nature (London)* **570**, 205 (2019).
- [70] A. Tononi, Y. M. Wang, and L. Salasnich, *Phys. Rev. A* **99**, 063618 (2019).
- [71] A. Rahmani and S. Vishveshwara, *Phys. Rev. B* **97**, 245116 (2018); Y. C. Wang, L. Zhang, S. Niu, D. P. Yu, and X. J. Liu, *Phys. Rev. Lett.* **125**, 073204 (2020).
- [72] Y. V. Kartashov, V. V. Konotop, and F. Kh. Abdullaev, *Phys. Rev. Lett.* **111**, 060402 (2013).
- [73] V. E. Lobanov, Y. V. Kartashov, and V. V. Konotop, *Phys. Rev. Lett.* **112**, 180403 (2014).
- [74] M. Salerno and F. Kh. Abdullaev, *Phys. Lett. A* **379**, 2252 (2015).
- [75] G. Gligoric, A. Maluckov, L. Hadzievski, S. Flach, and B. A. Malomed, *Phys. Rev. B* **94**, 144302 (2016).
- [76] F. Kh. Abdullaev and M. Salerno, *Phys. Rev. A* **98**, 053606 (2018).
- [77] D. A. Zezyulin, R. Driben, V. V. Konotop, and B. A. Malomed, *Phys. Rev. A* **88**, 013607 (2013).